8.1.2.4 Tilleyite, hemimorphite, wöhlerite and related silicates

The sorosilicates from groups VIIIB06 - VIIIB08 are listed in Table 1 [91N1]. Some authors use also the name of wöhlerite group, particularly for the VIIIB08 group of minerals [74A1].

8.1.2.4.1 Crystal structures. Lattice parameters

Cuspidine, $Ca_4Si_2O_7(F,OH)_2$

Cuspidine crystallizes in a monoclinic structure [55S1, 61W1] having space group $P2_1/a$ [74A1, 77S1].

Tilleyite, $Ca_5Si_2O_7(CO_3)_2$

The first crystal structure determination [53S1] was improved later [63B1]. A detailed analysis of the structure was reported by [70L1]. The silicate crystallizes in a monoclinic structure having the space group $P2_1/a$. The ***c***-axis projection of the tilleyite structure, in which Si_2O_7 groups are seen end-on as triangles, and each pair of CO_3 groups superimposes as the single triangle, is shown in Fig. 1 [70L1]. The atomic sites are listed in Table 2. Each CaO_4 column of octahedra superimposes in projection to yield the appearance of a single octahedron viewed down a diad axis. The corrugated walls of shared Si_2O_7 and CaO_4 groups lie parallel to {100}. Each wall consists of CaO_4 columns sharing edges with adjacent pairs of columns and sharing corners with Si_2O_7 groups. The corrugated walls are cross-linked by CO_3 groups sharing corners and edges with the CaO_4 columns and by a further type of CaO_4 column sharing corners with the other structural units. The above description of the structure is idealized [70L1]. To a first approximation, all atoms, except O13 occur in pairs displaced by about *c*/2. The exception, O13, is the bridging oxygen of the Si_2O_7 group and has no equivalent. In addition, the pairs of Si atoms are only 3.2 Å apart compared to *c*/2 = 3.8 Å. All of the CaO6 octahedra occur in pairs sharing edges to produce columns of CaO_4 composition lying parallel to ***c*** with a pseudo repeat of *c*/2. In addition to the pseudo-halving along ***c***, there is a pseudo-orthorhombic geometry. There is a further idealisation. The coordination polyhedra of Ca2 and Ca3 atoms are shown as distorted octahedra. Actually, each of these Ca atoms has seven oxygen neighbors at 2.3…2.7 Å. Although the six atoms ascribed to each octahedron are closer than the rejected ones, all seven are sufficiently close that they must be considered as first neighbors for bonding purposes. The distortions from idealized cell were explained by: (a) the misfit between the idealized shapes of the Si_2O_7 group and CaO_4 columns of octahedra, (b) the shortening of edges shared between polyhedra as expected from electrostatic forces between charged ions [70L1].

Jaffeite, $Ca_6Si_2O_7(OH)_6$

Jaffeite, ideally $Ca_6Si_2O_7(OH)_6$, is the analogue of the phase $3CaO{\cdot}SiO_2{\cdot}1.5H_2O$, tricalcium silicate hydrate [89S1]. The silicate crystallizes in a hexagonal structure having space group $P\bar{3}$. Because both jaffeite and hillebrandite, $Ca_2SiO_4{\cdot}H_2O$ (see section 8.1.1.7, subvol. 27I1) occur in the system $CaO\text{-}SiO_2\text{-}H_2O$, their coexistence in an apparent state of equilibrium is constrained by the phase relations in that system. These relations were determined under low-pressure hydrothermal conditions [62R1] or at high H_2O pressure [67R1]. They showed that both forms may coexist up to approximately 350°C. At that temperature, hillebrandite is replaced by reinhardbraunsite, $Ca_5(SiO_4)_2(OH,F)_2$ [83H1]. Jaffeite was found to form up to approximately 525°C, where it, too, decomposes to calciochondrodite, $Ca_5(SiO_4)_2(F,OH)_2$ plus fluid. In [67R1] was shown that jaffeite and hillebrandite can form together between 175 and 235°C at high H_2O pressure. Jaffeite remains stable above 500°C under high p_{H_2O} conditions. In [89S1] for jaffeite was suggested a temperature of formation less than 350°C, under hydrous conditions, in a system with relatively low silica activity.

Suolunite, $Ca_2Si_2O_5(OH)_2{\cdot}H_2O$

Suolunite, $Ca_2Si_2O_5(OH)_2{\cdot}H_2O$, crystallizes in an orthorhombic-type structure having space group Fdd2 [65H1, 68F1].

Hemimorphite $Zn_4Si_2O_7(OH)_2 \cdot H_2O$

The crystal structure of hemimorphite was analysed by various groups [32I1, 60B1, 67M1, 77H1, 78T1]. The silicate crystallizes in an orthorhombic-type structure, having space group Imm2. The structure consists of three-membered rings of corner-sharing $Zn(OH)O_3(x2)$ and SiO_4 tetrahedra arranged in compact sheets parallel to (010) - Fig. 2a [77H1]. Three oxygen atoms in each tetrahedron are bonded to two zinc atoms and one silicon atom,while a fourth oxygen atom forms a bridging bond to an equivalent cation in an adjacent sheet. The cross-bridging of the sheets produces additional rings of four, six and eight tetrahedra and forms a series of large cavities connected along the ***c***-axis. The water molecules near the centers of these cavities (in the plane of eightfold rings) are oriented parallel to (010) and are held in place by hydrogen bonds to the hydroxyl groups - Fig. 2b. The H atoms of the OH groups point towards the O atoms of the water molecule; thus they are also aligned parallel to (010). The atomic coordinates are given in Table 2. According to [77H1], on heating, it is apparent that the H_2O molecule is able to pass through the six-membered ring into an adjacent (vacanted) cavity above or below it, in the ***c***-axis direction, without disruption of the structure.

Upon heating, the water molecules are continuously lost between 393 and 657°C, whereas loss of hydroxide groups and breakdown of the structure occur at 740°C [51F1]. Above this temperature, anhydrous β-Zn_2SiO_4 is formed which transforms into willemite at 971°C [78G1]. The phase relations of these high-temperature products were investigated [62T1]. Hydrothermal experiments [56R1] showed that the upper stability limit of hemimorphite is ~ 250°C at 2…3 kbar, above which willemite +H_2O is stable. There is a contraction of the structure and the channels upon expulsion of the water molecules. A positive thermal expansion is observed in the dehydrated form – Table 3. The structural mechanism of contraction is dependent upon the collapse of the cavities interconnected parallel to ***c*** towards the position of the expelled water molecule. The decrease in the unit cell volume, ΔV_v, is directly correlated with volume loss in the cavities, ΔV_c, and the increase in volume of the Zn tetrahedra, ΔV_z: $\Delta V_v \cong 8\,\Delta V_c + 2\,\Delta V_z$ [81C1].

A possible dynamic disorder-order phase transition at low temperatures was tested by the determination of birefringence values (Δn) of hemimorphite between 82 and 373 K [97L1]. A strong discontinuity in the slope of $\Delta n_{X,Y}$ and $\Delta n_{Y,Z}$ was observed at 98(2)K – see section 8.1.2.4.3. This, together with considerable energy shifts of IR bands upon cooling provides evidence for a low-temperature second-order phase transition. In case of dehydrated hemimorphite, $Zn_4Si_2O_7(OH)_2$, no evidence of this type of transition was shown [97L2]. This was explained by the lack of an additional proton acceptor (O53 of the water molecule in hemimorphite) in the dehydrated phase.

Bertrandite

The crystal structure of bertrandite was originally solved by [65S1] and then refined by X-ray diffraction [86H2] and neutron diffraction [87D1] studies. The silicate crystallizes in space group $Cmc2_1$.

Junitoite, $CaZn_2Si_2O_7 \cdot H_2O$

According to [76W1], junitoite, $CaZn_2Si_2O_7 \cdot H_2O$, crystallizes in an orthorhombic structure having space group Bbm2. Later on, the structure was analysed in the space group Ama2 [85H1] (with interchanged *a* and *b* lattice constants of [76W1]). Zinc occurs in ZnO_4 tetrahedra which share corners to form continuous ZnO_3 chains along [010]. The chains are linked in the [001] direction by silicon tetrahedra, each of which is a member of an Si_2O_7 disilicate group to form zinc silicate sheets parallel to (010). These sheets join through the bridging oxygens of the disilicate group along ***a*** to form a three-dimensional tetrahedral framework. There are two sets of zinc tetrahedra slightly distorted and not identical. Ca occurs in distorted $CaO_5(H_2O)$ octahedra. Structurally, junitoite is closely related to hemimorphite. Both junitoite and hemimorphite [67M1] contain highly articulated ZnO_3 tetrahedral chains bridged by Si_2O_7 disilicate groups to form a three-dimensional tetrahedral network. In hemimorphite the network is compact except for channels along 1/2, 0, *x* and 0, 1/2, *z* which connect cavities at $z = 0$ and 1/2 which contain the water molecules. In junitoite the network forms large isolated cavities elongated along ***c***. These cavities contain the Ca in octahedral coordination and the water molecule [85H1].

Låvenite, wöhlerite, niocalite, hiortdahlite

The compositions of the above silicates can be derived from that of cuspidine $X_4[Si_2O_7](O,OH,F)_2$ where X = Ca or another metallic cation. Thus, the general formula may be written as $(X_LX_S)_4[Si_2O_7](O,OH,F)_2$ where X_L represents relatively large ions and X_S represent relatively small ions [74A1]. The crystal structures of the above silicates are listed in Table 4. Cuspidine is also included there. This silicate has the maximum symmetry because all its metallic cations are calcium and therefore have the same size [62S1]. Låvenite [63B1, 66F1, 66P1] retains the same symmetry because its ratio of relatively large to relatively small cations is close to unity. Wöhlerite displays lower symmetry because the ratio rises to about 3:1. Niocalite has an even greater unbalance of large and small cations. Some of the sodium in wöhlerite appears to be replaced by rare-earths (R) in hiortdahlite. Due to the larger ionic radii of R ions compared to the sodium or calcium ones, there is a tendency to crowd the neighboring sites making them too small to accommodate other ions. In addition, the R ions have higher positive charge than sodium and calcium. Fewer cations are therefore required to maintain the charge balance. The cationic deficiency and high ratio of large to small cations reduce the symmetry of hiortdahlite to P1 or $P\bar{1}$ [74A1].

The presence of pseudosymmetry (pseudo-orthorhombic B-face centered lattice) has been reported in the above silicates. In [66P1] the authors were misled by choosing an orthorhombic cell for låvenite in preference to a monoclinic cell, and in [57K1] similarly was chosen an orthorhombic cell for niocalite. Later on, it has been pointed out that both silicates are monoclinic and that the pseudo-orthorhombic character is the result of twinning [58N1, 61N1]. The pseudo-orthorhombic symmetry for låvenite and niocalite is compared in Table 3. In [74A1] the presence of pseudo-orthorhombic B-face centered lattice was shared for some natural hiortdahlites – Table 3. In addition to the pseudo-orthorhombic symmetry the natural hiortdahlite (Canada) display pseudo-monoclinic symmetry because of closeness of α and γ to 90°. The same pseudo-monoclinic symmetry is also apparent for niocalite [58N1]. The space group assigned to niocalite is Pa or P2/a [58N1]. The *a* glide plane manifests itself, in single crystal pattern, by the condition *hol*, present only when *h* is even. Despite its triclinic symmetry, hiortdahlite simulates this condition by the fact that when *h* is odd, the [*hol*]* rows are either absent or very weak, suggesting that the *a* glide plane is almost realised in the hiortdahlite structure, emphasising the pseudo-monoclinic character [74A1].

For crystal structures see also: låvenite [66F1, 66P1, 81M1]; wöhlerite [79M1, 89M1]; niocalite [66L1].

Komarovite, $(Ca,Mn)Nb_2Si_2O_9(O,F)\cdot 3.5H_2O$

Komarovite, $(Ca,Mn)Nb_2Si_2O_9(O,F)\cdot 3.5H_2O$, crystallizes in an orthorhombic unit cell [71P1, 77F1]. For Na-Komarovite see [79K1].

Mongolite, $Ca_4Nb_6Si_5O_{24}(OH)_{10}\cdot 6H_2O$

Mongolite, $Ca_4Nb_6Si_5O_{24}(OH)_{10}\cdot 6H_2O$, crystallizes in a tetragonal-type lattice [85V1, 86H1].

Janhaugite, $Na_3Mn_3(Ti,Zr,Nb)_2(Si_2O_7)_2O_2(OH,F)_2$

Janhaugite, $Na_3Mn_3(Ti,Zr,Nb)_2(Si_2O_7)_2O_2(OH,F)_2$ crystallizes in a monoclinic-type structure having space group $P2_1/n$ [83R1].

Baghdadite ($Ca_3ZrSi_2O_9$);$Ca_3HfSi_2O_9$

The $Ca_3MSi_2O_9$ with M = Zr, Hf silicates crystallize in monoclinic-type structure, having space group $P2_1/c$ [95P1]. The structure of $Ca_3ZrSi_2O_9$ contains ribbons of edge-sharing CaO_6 and ZrO_6 octahedra. The long direction of the ribbons is parallel to [100] and the width spans four octahedra. The ZrO_6 octahedra are in the middle of the ribbons and alternate with CaO_6 octahedra parallel to [100]. The ZrO_6 octahedra have a common edge almost parallel to (010) and are related by an inversion center - Fig. 3 [95P1]. A given ribbon touches (and shares oxygen with) two other ribbons at either end of its width. The touching ribbons diverge at an angle approximately 48° leaving narrow channels along [100]. In this channel trigonal prisms can be observed. Inserting in the prisms a nonlinear Si_2O group, a pyrosilicate group, Si_2O_7, with a trigonal prism outline is formed. Only alternate prisms can be occupied. The atomic coordinated are given in Table 2. The structure shows close relation with that of cuspidine [77S1] and låvenite [81M1]. However, while the space group is the

same and the axes are very similar, the monoclinic angle β differs from that of the mentioned structures by approximately 20°. Furthermore, the ZrO_6 octahedra in låvenite do not share edges. The natural mineral baghdatite, with the composition $Ca_3(Zr_{0.89}Ti_{0.11})(Si_{1.98}Fe_{0.01})O_9$, has a similar structure [86A1].

The atomic parameters of $Ca_3HfSi_2O_7$ are in good agreement with the atomic parameters of $Ca_3ZrSi_2O_7$. This may be correlated with almost identical ionic radii of Zr^{4+} and Hf^{4+} [95P1].

8.1.2.4.2 Nuclear magnetic resonance (NMR) data

Jaffeite, $Ca_6Si_2O_7(OH)_6$

^{29}Si NMR spectra were measured using the cross polarisation double-resonance technique in $Ca_6Si_2O_7(OH)_6$ [81G1]. In this system, obtained by the molybdate-reaction method, an impurity of monosilicate anions SiO_4^{4-}, in addition to the expected disilicate anions, $Si_2O_7^{6-}$, was shown [74W1]. The ^{29}Si spectrum exhibits a maximum and two shoulders in the low-field part - Fig. 4a. This line shape results from the overlapping of two components suggested by the dotted curve. The asymmetric line shape of the main component (91 % of the total intensity) indicates the axial symmetry of the corresponding chemical shift tensor ($\delta_\perp = -109$ ppm (maximum), $\delta_\parallel = -35$ ppm (shoulder)). The additional shoulder at -70 ppm is caused by the second component with nearly symmetric line shape, indicating the small axial symmetry of the corresponding chemical shift tensor. The more intense component with high shielding anisotropy, $\Delta\sigma = \sigma_\parallel - \sigma_\perp = -74$ ppm , was ascribed to the dimer silicate anions - Table 5. The less intense component with smaller anisotropy is attributed to the monomer anions. The isotropic chemical shift of the impurity corresponds to the isotropic value of calcium monosilicate, $Ca_2[HSiO_4|OH]$, $\delta = -72.5$ ppm [80L1]. A pictorial representation of the shielding tensor, using the shielding ellipsoid is given in Fig. 4b. The position of the principal tensor axes related to the Si–O bond frame shows that the shielding of the ^{29}Si atoms and the nature of the oxygen arrangement around the Si atom can be correlated. The pressed shielding ellipsoid ($\Delta\sigma$ negative) corresponds to the "pressed" tetrahedron of the SiO_4 end groups. The arrangement of the four Si–O bonds in SiO_4 tetrahedra is reflected by the ^{29}Si shielding tensor. The most shielded direction corresponds to the shortest Si-O bond [81G1].

The ^{29}Si NMR study on hemimorphite shows the presence of one Si site. The isotropic chemical shift is $\delta_I = -80$ ppm [83S1].

8.1.2.4.3 Optical properties

Hiortdahlite, niocalite, wöhlerite

The cathodoluminescence (CL) spectra from natural wöhlerites consist of a very broad emission that spans the entire visible spectrum and peaks in the blue-green at approximately 475 nm [89M1] - Fig. 5. Superimposed on this pattern is a narrower band that peaks at about 500 nm and was attributed to Mn^{2+} activation. The broad sweeping band was assumed to be intrinsic and probably associated with impurities affecting the Si–O bonds. It may be enhanced by the presence of Ti.

The natural niocalite spectrum shows line emission from Sm^{3+} at 600 nm, 650 nm and a small unlabeled peak at 700 nm. The presence of Sm^{3+} activation reflects the light rare-earth dominance of carbonatite environments. In contrast, for natural hiortdahlite the major activator is Dy^{3+} with line emission at 485 nm and 575 nm. In addition, the strongest emission of Tb^{3+} also is resolved at 550 nm. The broad bands at 600 nm and 650 nm probably are due to multiple unresolved emission from Sm^{3+} and Mn^{2+}, or they may be a result of rare-earths peak overlap. The hiortdahlite spectrum with peaks due to Dy^{3+} and Tb^{3+} reflects heavy rare-earth dominant activation. The variable intensity of CL spectra among different wöhlerite samples is mainly a function of the ability of iron to quench CL emission [89M1].

Hemimorphite

The polarized IR absorption spectra of oriented hemimorphite single crystal where recorded in the region of O–H fundamentals and combination bands as function of temperature [97L1]. The stretching and bending modes of

the H_2O and OH groups of hemimorphite, parallel to the crystallographic axes, are shown in Fig. 6 [97L1]. At ambient and elevated temperatures the O–H stretching region consists of superimposed broad absorption bands around 3400…3650 cm^{-1} in the ***a*** direction and around 3200…3550 cm^{-1} in the ***c*** direction. At low temperatures, the single components of the broad stretching bands are resolved. The H_2O bending mode in the ***c***-spectrum is sharp at all temperatures. The almost exclusive orientation of the absorption bands in the (010) plane is in agreement with neutron diffraction study [77H1]. The weak H bonds of the OH groups and water molecules were confirmed by the energies of the OH stretching bands around 3350…3600 cm^{-1}. Two O–H stretching bands in both ***a*** and ***c***-spectra were predicted by factor group analysis, but three strong bands in ***a*** and two in ***c*** were observed. This fact, as well as the occurrence of weak satellite bands in the ***a*** and ***c***-spectra and a minor component parallel to the ***b***-axis direction, indicate complicated dynamics of the water molecules and OH groups within the structure channels. These motions can be partly explained by a twisting motion of the water molecule around its twofold molecular axis. A better interpretation for these motions was found in dynamic proton disorder, which describes a hopping motion between disordered proton sites.

The polarized single crystal IR spectra for dehydrated hemimorphite are shown in Fig. 7 [97L2]. Only the OH stretching region in a 7 µm thick (010) slab parallel to ***a*** and ***c*** was shown since the polarization direction parallel to ***b*** did not show any OH absorption. The strongest absorption band is observed in the ***a*** spectra at 3516 (82 K) to 3535 cm^{-1} (373 K). The exclusive appearance in ***a*** type spectra indicates an OH vector direction parallel to ***a***. Weaker absorption were observed in the ***a*** and ***c*** spectra at 3603 cm^{-1}. The slightly different intensities in ***a*** (~ 10 cm^{-1}) and ***c*** (~ 12 cm^{-1}) spectra indicate an OH vector orientation between the two axes, with preference toward ***c***. The IR and X-ray studies show that the protons of the hydroxide groups are disordered in the structural channels. One proton is located at the line between two O3 atoms (O3-O3') thus building up a weak H bond. The corresponding O-H stretching band occurs at ~ 3530 cm^{-1} and is polarized parallel to ***a***. Due to proton-proton repulsion, the O-H vector of the other H atom deviates from the O3-O3' line. As a consequence, the corresponding IR stretching vibration is observed at ~ 3600 cm^{-1} and components of this band occur parallel to ***a*** and ***c***.

The birefringence values, Δn, of hemimorphite were determined in the temperature range 82 K…373 K [97L1]. In (010) slabs a constant birefringence, $\Delta n_{Y,Z} = 0.0186(2)$ at a wavelength of 490 nm ($Y \parallel \boldsymbol{a}$, $Z \parallel \boldsymbol{c}$) is observed between 100 and 373 K, whereas the $\Delta n_{X,Y}$ values in (001) decrease from 0.005 at 100 K to below 0.003 at room temperature. A discontinuity in birefrigence curves was shown at 98(2) K - Fig. 8. The strong shifts of IR stretching bands with changing temperature provide an additional support for an order-disorder transition. In case of dehydrated hemimorphite the temperature dependence of birefringence shows smooth curves which do not indicate a transition [97L2].

Janhaugite

The infrared spectrum of janhaugite is plotted in Fig. 9 [83R1]. The relatively sharp O-H stretching frequencies at 3550, 3510 and 3460 cm^{-1} are present. Small absorption due to H_2O bending vibrations occur at 1640/1620 cm^{-1}. The SiO_4 tetrahedra give strong absorption in the region 1080…870 cm^{-1}. Band assignments at lower frequencies were more difficult. A spurious band occurs at 1375 cm^{-1}.

The refractive indices for some silicates are given in Table 6.

Tables and figures

Table 1. Sorosilicates from groups VIIIB06 – VIIIB08 [91N1].

Silicate	Composition	Group
Cuspidine	$Ca_4Si_2O_7(F,OH)_2$	VIIIB06
Tilleyite	$Ca_5Si_2O_7(CO_3)_2$	VIIIB06
Jaffeite	$Ca_6Si_2O_7(OH)_6$	VIIIB06
Suolunite	$Ca_2Si_2O_5(OH)_2 \cdot H_2O$	VIIIB06
Killalaite	$Ca_3Si_2O_7 \cdot H_2O$	VIIIB06
Junitoite	$CaZn_2Si_2O_7 \cdot H_2O$	VIIIB07
Hemimorphite	$Zn_4Si_2O_7(OH)_2 \cdot H_2O$	VIIIB07
Bertrandite	$Be_4Si_2O_7(OH)_2$	VIIIB07
Låvenite	$Na_2(Mn,Ca,Fe)(Zr,Nb)Si_2O_7(O,OH,F)_2$	VIIIB08
Wöhlerite	$Ca_4Na_2ZrNb(Si_2O_7)_2(O,OH,F)_4$	VIIIB08
Niocalite	$Ca_7Nb(Si_2O_7)_2O_3F$	VIIIB08
Hiortdahlite I	$Na_4Ca_8Zr_2(Nb,Mn,Ti,Fe,Mg,Al)_2(Si_2O_7)_4O_3F_5$	VIIIB08
Hiortdahlite II	$(Na,Ca)_4Ca_8(Y,Na)_2Zr_2(Si_2O_7)_4O_3F_5$	VIIIB08
Komarovite	$(Ca,Mn)Nb_2(Si_2O_7)(O,F)_3 \cdot 3.5\ H_2O$	VIIIB08
Na-Komarovite	$(Na,Ca,H)_2Nb_2Si_2O_{10}(OH,F)_2 \cdot H_2O$	VIIIB08
Mongolite	$Ca_4Nb_6Si_5O_{24}(OH)_{10} \cdot 6\ H_2O$	VIIIB08
Janhaugite	$Na_3Mn_3(Ti,Zr,Nb)_2(Si_2O_7)_2O_2(OH,F)_2$	VIIIB08
Baghdadite	$Ca_3ZrO_2(Si_2O_7)$	VIIIB08

Table 2. Atomic coordinates and temperature factor coefficients

a) Tilleyite having monoclinic-type structure of space group $P2_1/a$ [70L1].

Atom	x	y	z	B_{eq} [Å^2]
Ca1	0.0033(1)	0.9938(2)	0.7501(3)	0.75(2)
Ca2	0.1769(1)	0.2135(2)	0.0908(2)	0.69(2)
Ca3	0.1813(1)	0.2064(2)	0.6087(2)	0.79(2)
Ca4	0.1239(1)	0.5895(2)	0.0449(2)	0.62(2)
Ca5	0.1359(1)	0.5787(2)	0.5599(2)	0.72(2)
Si1	0.2032(1)	0.9209(2)	0.1381(3)	0.42(3)
Si2	0.2023(1)	0.9142(2)	0.5689(3)	0.57(3)
C1	0.0301(6)	0.3058(9)	0.3402(11)	1.14(12)
C2	0.0248(6)	0.3018(9)	0.8157(11)	0.84(11)
O1	0.0752(5)	0.2048(8)	0.2983(10)	1.10(10)
O2	0.0713(5)	0.2052(8)	0.7867(10)	1.08(10)
O3	0.0705(4)	0.3772(7)	0.4807(9)	1.08(10)
O4	0.0547(4)	0.3766(7)	0.9563(9)	1.01(9)
O5	0.0519(5)	0.6642(7)	0.7549(10)	1.37(10)
O6	0.0584(5)	0.6826(7)	0.2834(10)	1.25(11)
O7	0.2253(4)	0.7744(7)	0.0878(8)	0.73(12)
O8	0.2272(5)	0.7665(7)	0.6290(8)	0.81(9)
O9	0.1008(5)	0.9760(8)	0.0528(9)	0.98(9)
O10	0.1018(4)	0.9711(7)	0.5524(9)	0.83(9)
O11	0.2263(4)	0.5308(6)	0.8839(8)	1.01(8)
O12	0.2214(4)	0.5219(6)	0.3202(8)	0.77(8)
O13	0.2253(4)	0.9161(7)	0.3639(8)	1.18(8)

Table 2 (continued)

b) Hemimorphite having orthorhombic-type structure of space group Imm2 [77H1].

Atom[1)]	x	y	z	$\beta_{ij} \cdot 10^4$					
				β_{11}	β_{22}	β_{33}	β_{12}	β_{13}	β_{23}
Zn	0.2047(1)	0.1613(1)	0	29(1)	20(1)	66(4)	–5(1)	–1(2)	3(2)
Si	0	0.1465(2)	0.5076(5)	23(2)	13(1)	45(6)	0	0	0(3)
O1	0.1602(2)	0.2055(1)	0.6362(4)	38(1)	26(1)	70(4)	–17(1)	9(2)	9(2)
O2	0	0.1669(2)	0.1938(4)	27(2)	33(1)	55(5)	0	0	4(2)
O3	0.3050(2)	0	0.0410(6)	50(2)	18(1)	271(10)	0	–30(4)	0
O4	0	0	0.5912(6)	54(3)	10(2)	124(9)	0	0	0
O5	0.5000	0	0.5195(13)	164(50)	227(12)	221(9)	0	0	0
H35	0.3740(8)	0	0.0190(2)	154(9)	56(4)	692(41)	0	–224(18)	0
H53	0.4256(14)	0	0.0643(4)	247(21)	247(18)	1163(101)	0	102(45)	0

[1)] The atoms of the H_2O group were denoted by H53(O5) and those of the OH group by H35(O3).

c) $Ca_3ZrSi_2O_9$ crystallizing in a monoclinic structure of $P2_1/c$ type [95P1].

Atom	x	y	z
Zr1	0.1245(8)	0.0629(4)	0.1148(5)
Ca1	0.6247(8)	0.8070(5)	0.5994(8)
Ca2	0.1198(9)	0.8256(5)	0.5884(6)
Ca3	0.6301(11)	0.4193(6)	0.6155(6)
Si1	0.8340(9)	0.6240(8)	0.8189(7)
Si2	0.4000(11)	0.6350(9)	0.8074(7)
O1	0.6176(7)	0.6058(5)	0.7757(4)
O2	0.0825(9)	–0.0033(6)	0.7541(5)
O3	0.1391(8)	0.3794(5)	0.0310(5)
O4	0.1069(10)	0.2634(5)	0.7432(5)
O5	0.3557(8)	0.7356(5)	0.2253(5)
O6	0.3119(6)	0.4990(6)	0.7603(5)
O7	0.3791(8)	0.6636(5)	0.9566(5)
O8	0.0976(6)	0.6113(5)	0.5056(5)
O9	0.6596(7)	–0.1090(6)	–0.0117(5)

Table 3. Crystal structures and lattice parameters.

Silicate	*T* [K]	Space group	Lattice parameters				Refs.
			a [Å]	*b* [Å]	*c* [Å]	α, β, γ	
Cuspidine[1)]	RT	$P2_1/a$	10.85	10.43	7.54	$\beta = 110°04'$	55S1
Cuspidine[1,1a)]	RT		10.93	10.57	7.57	$\beta = 110°06'$	61W1
Tilleyite[2)]	RT	$P2_1/a$	15.079(10)	10.241(4)	7.573(3)	$\beta = 105.14(3)°$	70L1
Tilleyite[3)]	RT	$P2_1/a$	15.111(5)	10.242(2)	7.577(2)	$\beta = 105.15(2)°$	70L1
Tilleyite[3)]	RT	$P2_1/a$	15.108(3)	10.241(1)	7.579(1)	$\beta = 105.17(1)°$	70L1
Jaffeite[4)]	RT	$P\bar{3}$	10.026(5)		7.482(4)		89S1
Suolunite[5)]	RT	Fdd2	11.15(3)	19.67(5)	6.08(2)		65H1, 68F1
Hemimorphite[6)]		Imm2	8.370	10.719	5.120		67M1
Hemimorphite[6)]	295	Imm2	8.367(5)	10.730(6)	5.115(3)		77H1
Hemimorphite[6)]	RT	Imm2	8.366(1)	10.714(1)	5.113(1)		78T1
Hemimorphite[6)]	295	Imm2	8.206(4)	10.815(6)	5.089(2)		81C1
	573	Imm2	8.337(5)	10.724(6)	5.116(4)		81C1
	873	Imm2	8.268(5)	10.784(8)	5.113(3)		81C1
Hemimorphite (dehydrated, natural,	110	Imm2	8.181(1)	10.841(6)	5.081(1)		97L1
Chihuohua, Mexico)	293	Imm2	8.191(1)	10.824(2)	5.088(1)		97L1
Junitoite[7)]	RT	Bbm2	6.309(6)	12.503(6)	8.549(6)		76W1
Junitoite, $CaZn_2Si_2O_7 \cdot H_2O$	RT	Ama2	12.510(7)	6.318(3)	8.561(6)		85H1
Bertrandite, $Be_4Si_2O_7(OH)_2$	RT	$Cmc2_1$	8.7135(4)	15.268(1)	4.5683(3)		87D1
Låvenite[8)]	RT	monoclinic	10.95	10.01	7.19	$\beta = 110°18'$	34G1
Låvenite[9)]	RT	pseudo-orth.	21.01(10)	10.05(5)	7.23(3)	$\alpha = 90°$ $\beta = 90°$ $\gamma = 90°$	66P1, 66F1
Wöhlerite[10)]	RT	monoclinic	10.87	10.27	7.32	$\beta = 109°05'$	58N1
Niocalite[11)]	RT	monoclinic	10.83	10.42	7.38	$\beta = 109°40'$	58N1
Niocalite[11)]	RT	pseudo-orth.	20.40	10.42	7.38	$\alpha = 90°$ $\beta = 90°30'$ $\gamma = 90°$	58N1
Hiortdahlite[12)]	RT	$P\bar{1}$ or P1	10.95(3)	10.31(2)	7.29(3)	$\alpha = 90°19(10)'$ $\beta = 109°02(15)'$ $\gamma = 90°05(10)'$	74A1
Hiortdahlite[13)]	RT		10.95	10.31	7.29	$\alpha = 90°19'$ $\beta = 109°02'$ $\gamma = 90°05'$	74A1
Hiortdahlite[14)]	RT	pseudo-orth.	20.70	10.31	7.30	$\alpha = 90°20'$ $\beta = 90°37'$ $\gamma = 89°47'$	74A1
Hiortdahlite[15)]	RT		10.93	10.31	7.33	$\alpha = 90°29'$ $\beta = 108°50'$ $\gamma = 90°08'$	34G1
Komarovite[16)]	RT	orth.	21.30(7)	14.00(5)	17.19(7)		71P1, 72F1
Mongolite[17)]	RT	tetrag.	7.00(5)		29.0(1)		85V1, 86H1
Janhaugite[18)]	RT	$P2_1/n$	10.668(2)	9.787(4)	13.931(3)	$\beta = 107.82(2)°$	83R1
Baghdadite[19)]	RT	$P2_1/a$	10.42(2)	10.16(2)	7.36(1)	$\beta = 91.1°$	86A1, 87H1
$Ca_3HfSi_2O_9$	RT	$P2_1/c$	7.3517(4)	10.1489(1)	10.4319(12)	$\beta = 91.084(7)°$	95P1
$Ca_3ZrSi_2O_9$	RT	$P2_1/c$	7.3603(1)	10.1766(3)	10.4514(3)	$\beta = 90.875(2)°$	95P1

[1)] lattice parameters setting in space group $P2_1/a$;
[1a)] obtained from the crushed slags which came from furnaces fed with fluorine containing phosphate rock;

Table 3 (continued)

[2] synthetic $Ca_5Si_2O_7(CO_3)_2$; [3] natural silicates; [4] $Ca_{5.86}Si_{2.02}O_{13}H_{6.21}$;
[5] $Ca_2H_2Si_2O_7 \cdot H_2O$ (SiO_2 43.8, CaO 42.95, H_2O 13.17, K_2O, Na_2O, SrO traces; sum 99.50, corresponding to $CaSiO_3 \cdot H_2O$);
[6] $Zn_4Si_2O_7(OH)_2 \cdot H_2O$; [7] $Ca_{0.98}Zn_{1.96}Si_{1.84}O_{6.6} \cdot 1.13\ H_2O$; [8] natural, Langesundsfjord, Norway;
[9] $(Na_{1.40}Ca_{1.10}Mn_{0.09}Fe^{2+}_{0.02}Fe^{3+}_{0.05}R_{0.10})(Zr_{0.98}Nb_{0.02}Ti_{0.10})Si_2O_7(O_{0.30}(OH)_{0.59}F_{1.30})$;
[10] natural, Langesundsfjord, Norway; [11] natural, Oka, Canada;
[12] $(Ca_{2.01}Na_{0.85}Y_{0.12}R_{0.04})(Zr_{0.58}Nb_{0.02}Mn_{0.02}Ti_{0.01}Fe_{0.01}Mg_{0.01}Al_{0.01})(Si_{2.05}O_7)(F_{1.34}O_{0.41}OH_{0.18})$;
[13] natural, Kipawa River, Quebec; [14] natural Sheffield, Quebec;
[15] natural, Langesundsfjord, Norway;
[16] $(Ca_{0.43}Mn_{0.36}Na_{0.14}K_{0.03})(Nb_{1.82}Ti_{0.16}Al_{0.16}Fe_{0.10})Si_2O_9(O_{0.88}F_{0.33}) \cdot 3.5\ H_2O$;
[17] $(Ca_{3.01}Na_{0.31}Sr_{0.28}K_{0.14}Ba_{0.06})(Nb_{5.45}Al_{0.22}Mn_{0.22}Zn_{0.07}Mg_{0.03})(Si_{5.00}O_{27.84}) \cdot 5.07\ H_2O$;
[18] $(Na_{2.75}Ca_{0.20}K_{0.03})(Mn_{2.43}Fe_{0.60})(Ti_{1.32}Zr_{0.38}Nb_{0.29}Ta_{0.01})(Si_{3.84}Ti_{0.15})O_{15}(OH_{1.40}F_{1.10}O_{0.50})$;
[19] $Ca_{3.00}(Zr_{0.89}Ti_{0.11})(Si_{1.98}Fe_{0.01})O_9$.

Table 4. The relationship of symmetry to the proportion of large (X_L) and small (X_S) cations [74A1].

Silicate	X_L	X_S	X_L/X_S	Space goup
Cuspidine	$Ca_{3.9}$	$(Al,Fe,etc)_{0.1}$	39/1	$P2_1/a$
Låvenite	$Na_{1.2}Ca_{1.0}$	$(Zr,Mn,Fe,Ti)_{1.7}$	1.3/1	$P2_1/m$
Wöhlerite	$Ca_{1.9}Na_{1.0}$	$(Zr,Nb)_{1.1}$	2.6/1	$P2_1$
Niocalite	$Ca_{3.4}$	$Nb_{0.7}$	4.9/1	$P2_1$, Pa or P2/a
Hiortdahlite	$Ca_{2.0}(Na,R)_{1.0}$	$Zr_{0.7}$	4.3/1	P1 or $P\bar{1}$

Table 5. ^{29}Si chemical shift in $Ca_6Si_2O_7(OH)_6$.

Anion	Symmetry	$\delta_{\parallel}$ [1] [ppm]	$\delta_{\perp}$ [ppm]	δ_{iso} [2] [ppm]	$\Delta\sigma$ [3] [ppm]	Ref.
$Si_2O_7^{6-}$	axial	–35(2)	–109(2)	–84(2)	–74(2)	81G1
$Si_2O_7^{6-}$				–82.6		80L1

[1] relative to TMS; [2] $\delta_{iso} = (2\delta_{\perp} + \delta_{\parallel})/3$; [3] $\Delta\sigma = -\Delta\delta = -(\delta_{\parallel} - \delta_{\perp})$.

Table 6. Refractive indices.

Silicate[a]	n_α (ω)	n_β	n_γ (ε)	$2V°$		Refs.
Cuspidine[1a]	1.590(2)	1.593(2)	1.602(2)	58°	biaxial positive	61W1
Jaffeite[4]	1.596(2)(ω)		1.604(2)(ε)		uniaxial positive	89S1
Junitonite[7]	1.656	1.664	1.672	86°		76W1
Låvenite[9]	1.645	1.652	1.656	86°		66F1,66P1
Hiortdahlite[12]	1.639(3)	1.643	1.646(2)	80°…83°		74A1
Komarovite[16]	1.750(20)	1.766(20)	1.85(2)	48°	biaxial positive	71P1,72F1
Janhaugite[18]	1.770(4)	1.828(4)	1.910 (calc.)	80(10)°	biaxial positive	83R1
Baghdadite[19]	1.652	1.658	1.670	72°	biaxial positive	86A1,87H1

[a] compositions are given in Table 3.

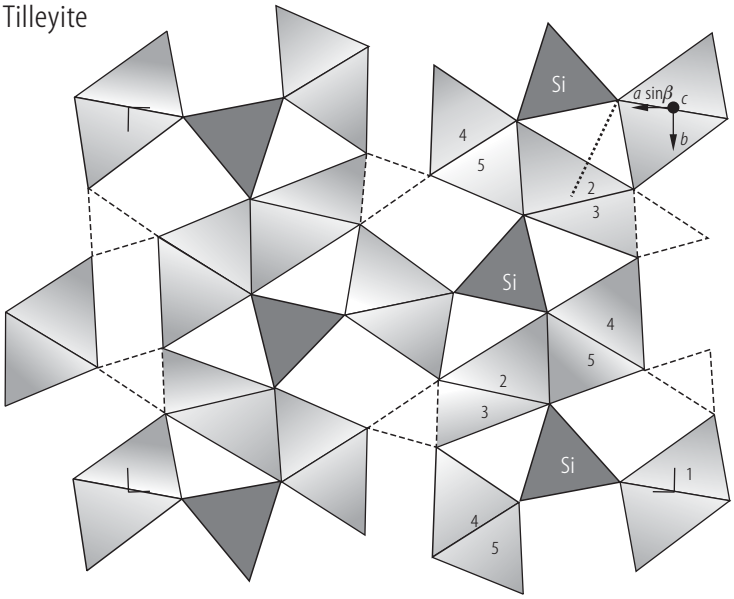

Fig. 1. Tilleyite. Idealized projection viewed down the ***c***-axis. The Si_2O_7 groups are represented end-on by the dark-shaded triangles. The CO_3 groups are shown by the broken-line triangles. The CaO_6 octahedra are viewed down a diad axis. The octahedra for the Ca2 and Ca3 atoms were obtained by omitting the seventh largest distance shown by the dotted lines. One of the corrugated sheets consists of Si_2O_7 and CaO_6 octahedra marked by Si, 2, 3, 4 and 5 [70L1].

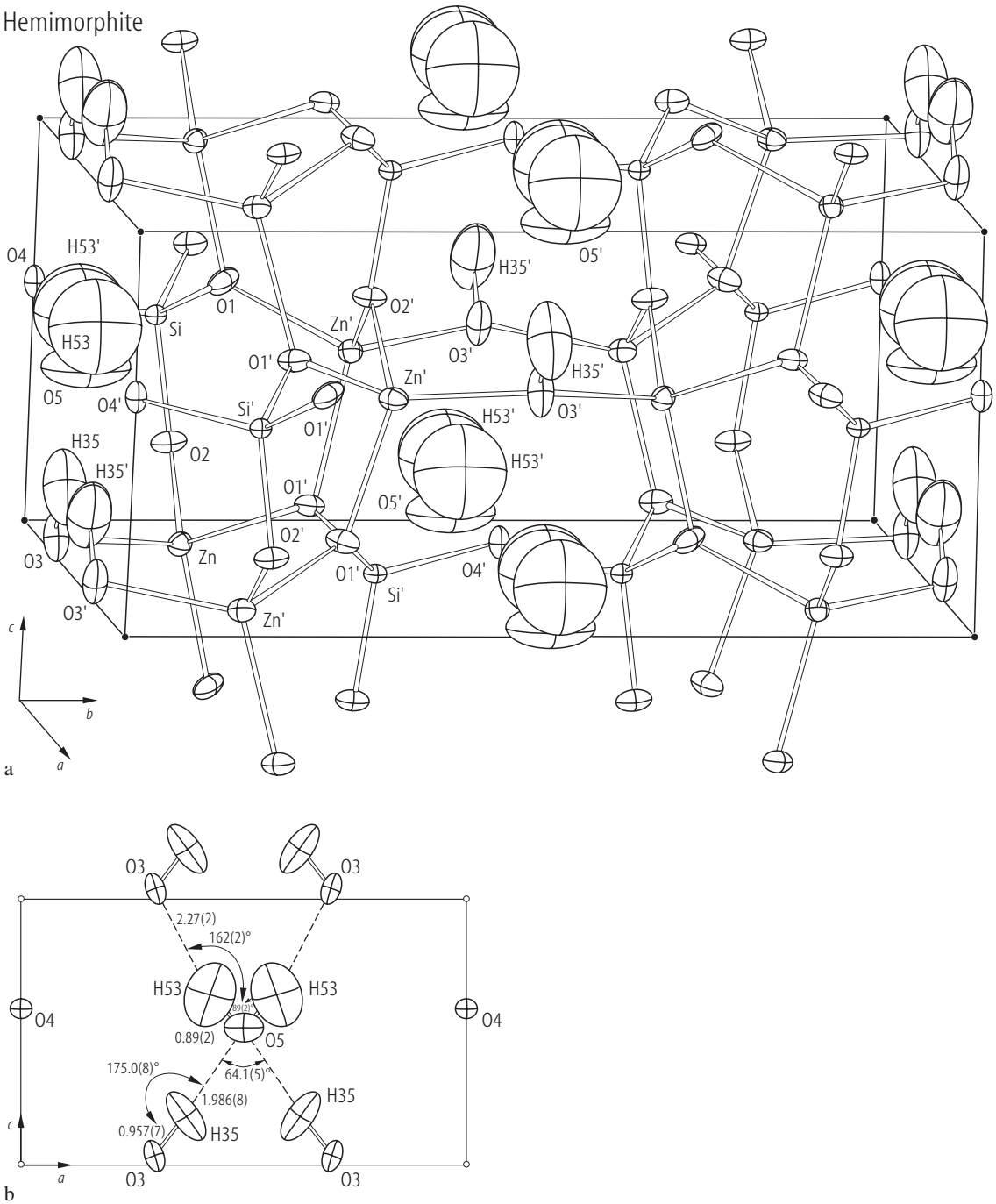

Fig. 2. Hemimorphite. **(a)** Crystal structure [77H1]. Atoms outside the asymmetric unit are labelled with superscript primes. **(b)** Section through the cavity at $y = 0$. Hydrogen bonds are indicated by dashed lines. Distances are in Å units. In **(a)** and **(b)** thermal ellipsoids for all atoms represent 50 % probability surfaces.

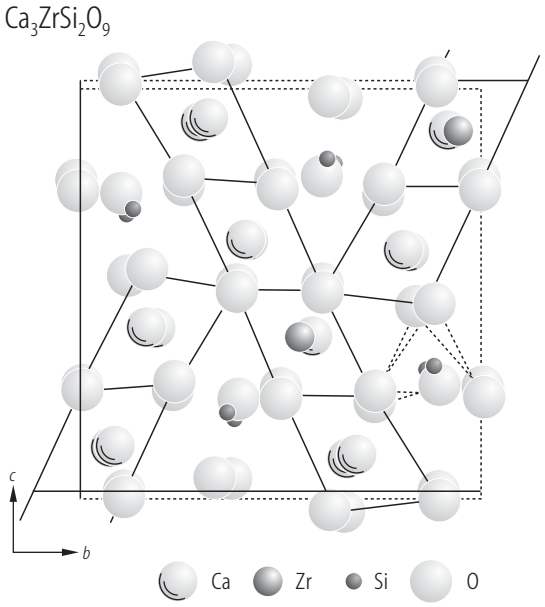

Fig. 3. $Ca_3ZrSi_2O_9$. Projection of the structure along the ***a***-axis [95P1].

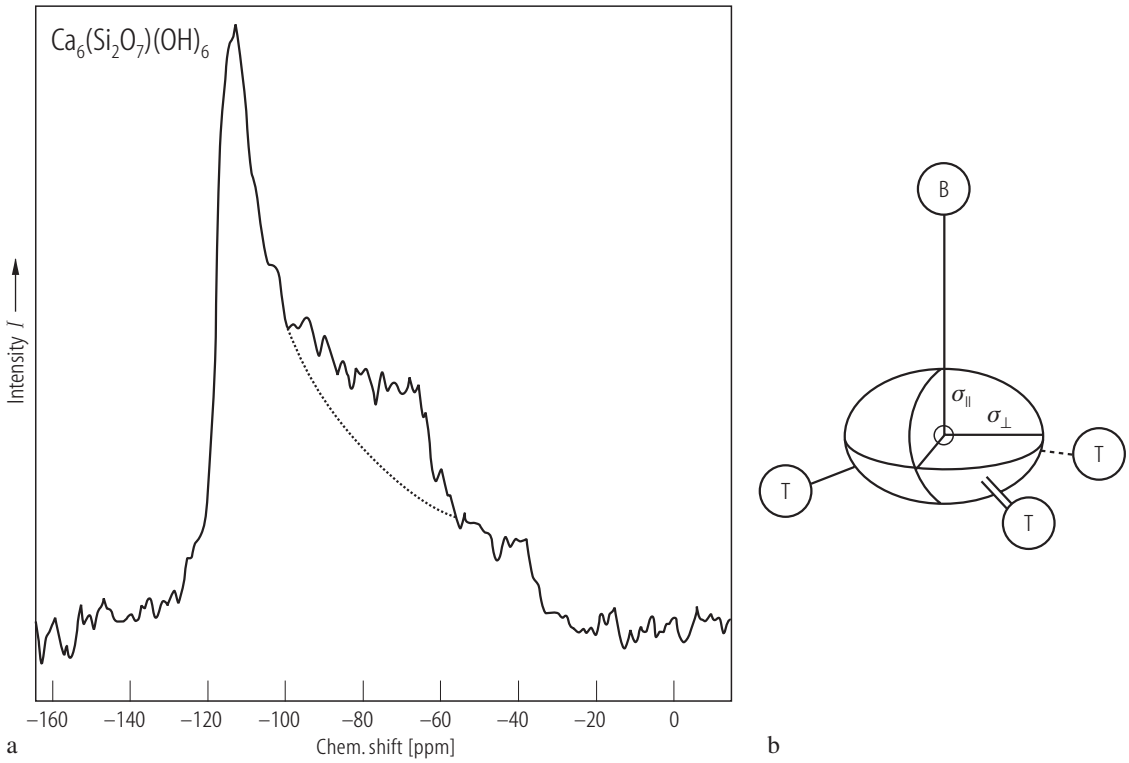

Fig. 4. $Ca_6Si_2O_7(OH)_6$. **(a)** ^{29}Si NMR spectrum, **(b)** pictorial representation of the orientation of the ^{29}Si shielding tensor [81G1]. T: terminal oxygen, B: bridging oxygen.

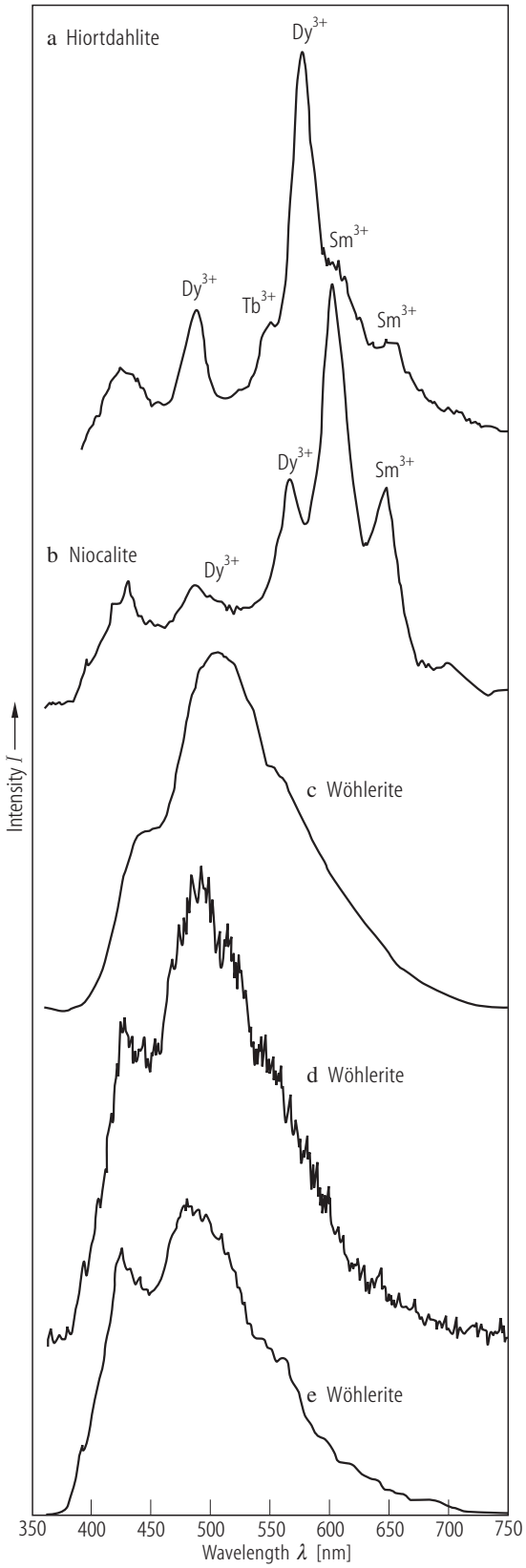

←

Fig. 5. Hiortdahlite natural (Kipawa, Quebec) **(a)**, Niocalite natural (Oka, Quebec) **(b)**, Wöhlerite **(c, d, e)**. Cathodoluminescence emission spectra [89M1]. Compositions are:
(c)
$Na_{4.01}(Ca,Fe,Mn,Mg)_{7.89}(Zr,Hf)_2(Nb,Ta,Ti)_{2.02}Si_{8.15}O_{34}(O,OH,F)$ with 1.65 F
(d)
$Na_{2.71}(Ca,Fe,Mn,Mg)_{8.17}(Zr,Hf)_{1.97}(Nb,Ta,Ti)_{1.96}Si_{8.16}O_{34}(O,OH,F)$ with 1.62 F
(e)
$Na_{3.96}(Ca,Fe,Mn,Mg)_{8.10}(Zr,Hf)_{1.94}(Nb,Ta,Ti)_{1.94}Si_{8.18}O_{34}(O,OH,F)$ with 1.82 F.

→

Fig. 6. Hemimorphite. Polarized FTIR absorption spectra [95L1]. The spectra were offset vertically by 0.8 each **(a)**, by 0.9 each **(b)**, by 1.1, 0.9 and 0.5 (***c*** stretching) and by 0.8 each (***c*** bending). Because the spectra of the ***b*** direction were measured on a comparably thicker slab than the ***a*** and ***c*** directions, the absorbance scale was compressed to allow for direct graphical comparison of intensities. The tiny zigzag lines on top of the bands represent noise enhanced by strong absorption. Asterisks around 1720 cm^{-1} mark organic impurities.

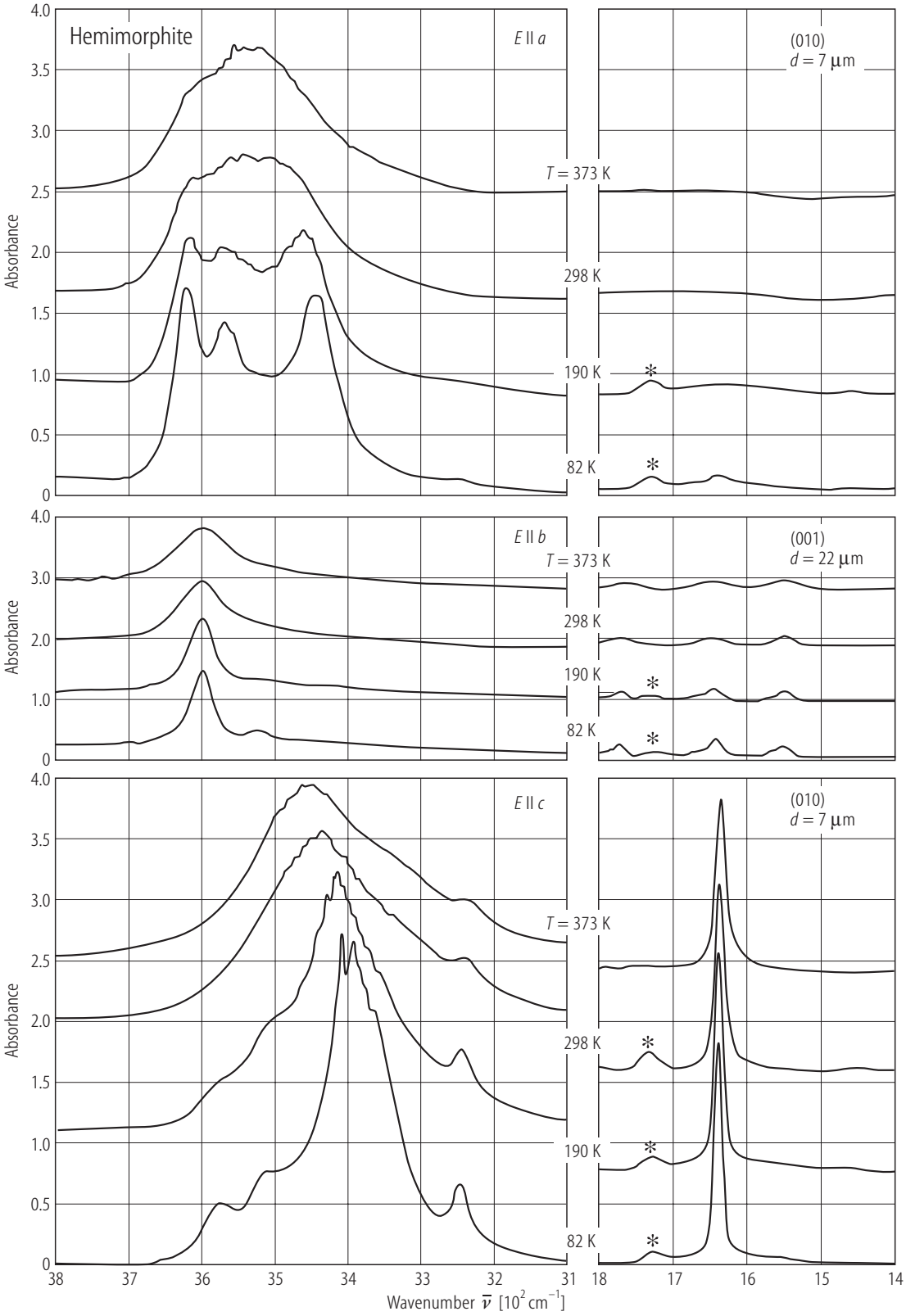
Hemimorphite
E II a
(010)
d = 7 μm
T = 373 K
298 K
190 K
82 K
E II b
(001)
d = 22 μm
E II c
(010)
d = 7 μm
Absorbance
Wavenumber ν̄ [10² cm⁻¹]

Fig. 6.

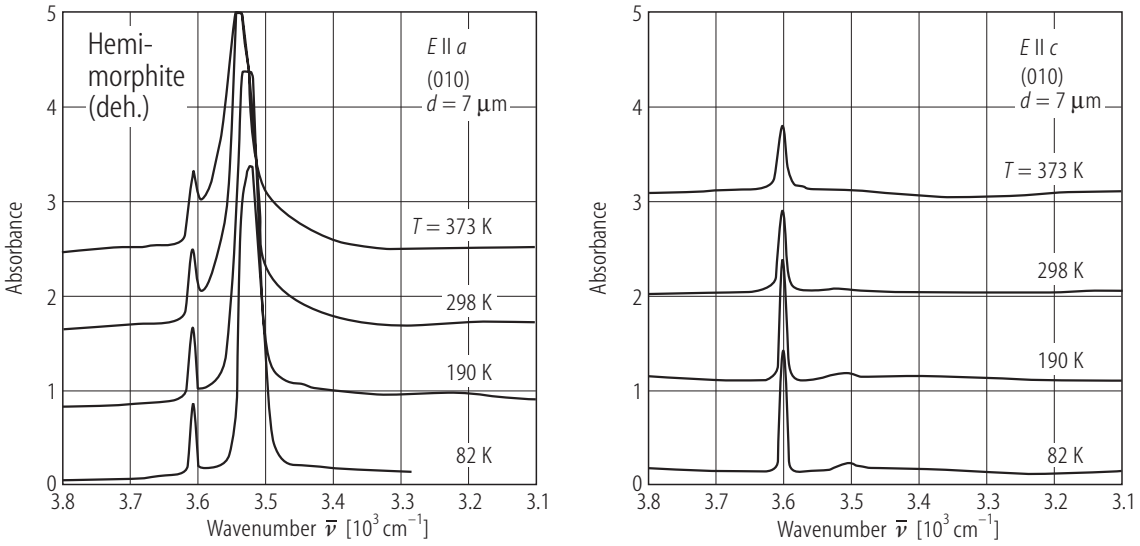

Fig. 7. Dehydrated hemimorphite. Polarized single crystal IR spectra of a 7µm thick (010) platelet [97L2]. Due to the intense absorption of the band around 3530 cm^{-1}, the peak is truncated. Spectra were vertically offset by 0.8 each (***a***-spectra) and by A = 1.0 each (***c***-spectra).

For Fig. 8 see next page

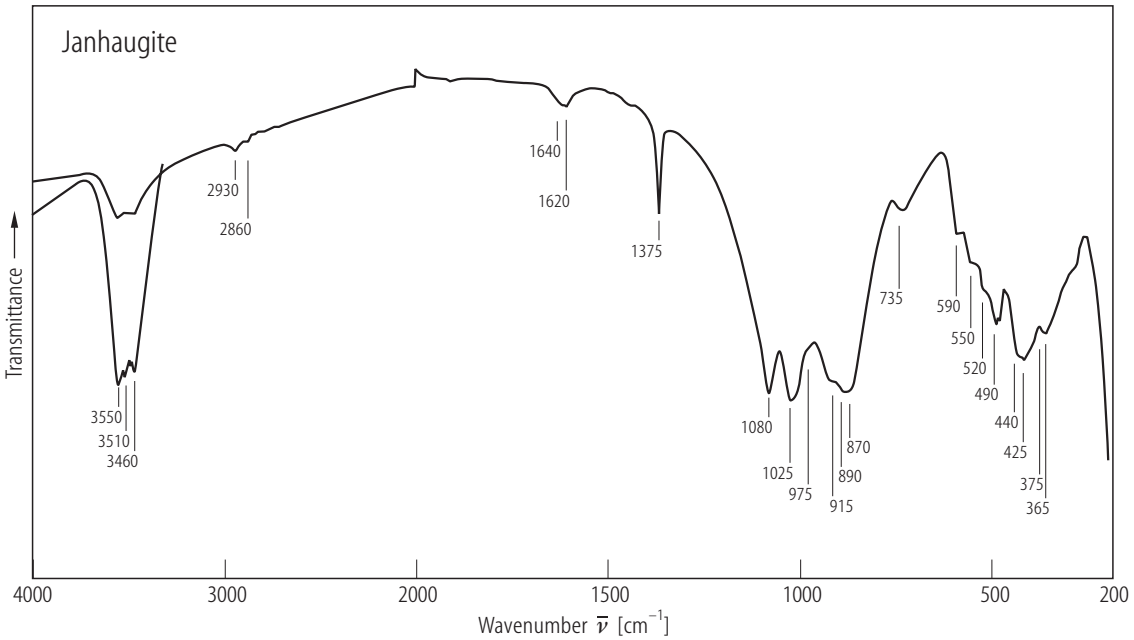

Fig. 9. Janhaugite. Infrared spectrum [83R1]. Composition is given in Table 3, footnote [18)].

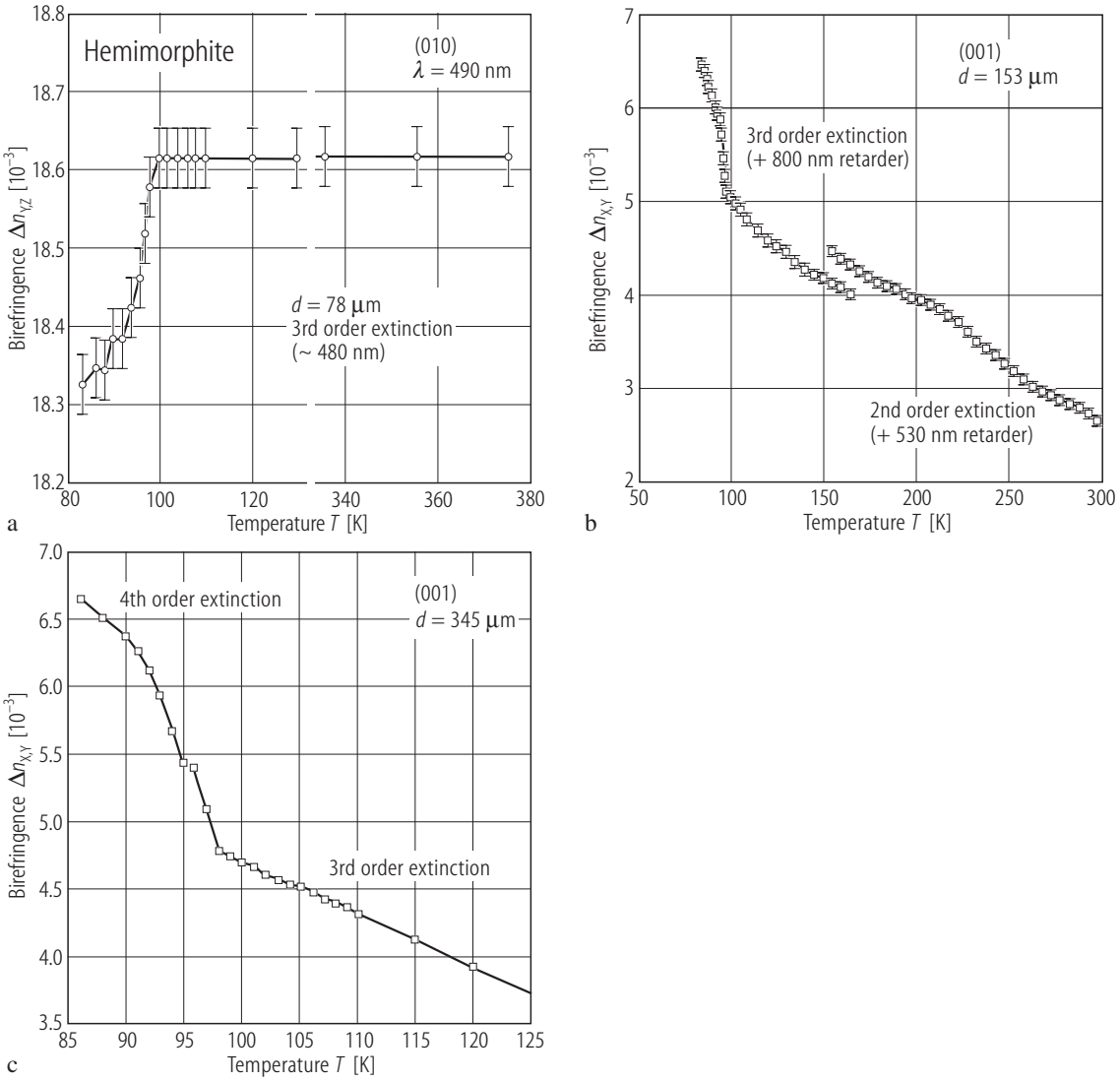

Fig. 8. Hemimorphite. Birefringence versus temperature [97L1] **(a)** (010) section; **(b)** (001); **(c)** (001) section. The breaks in the curves are caused by measuring procedure.

References for 8.1.2.4

32I1 Ito, T., West, J.: Z. Kristallogr.83 (1932) 1
34G1 Gossner, B., Kraus, O.: Zentralbl. Mineral. Geol. Palaelontol. Abt A (1934) 72
51F1 Faust, G.T.: Am. Mineral. 36 (1951) 795
53S1 Smith, J.V.: Acta Crystallogr. 6 (1953) 9
55S1 Smirnova, R.F., Rumanova, I.M., Belov, N.V.: Zap. Vses. Mineral. Ova. 84 (1955) 159, Abstr. in Zentralblatt Min. 1 (1956) 67
56R1 Roy, D.M., Mumpton, F.A.: Econ. Geol. 51 (1956) 432
57K1 Kern, R., Rimsky, A., Monier, J.C.: C. R. Acad. Sci. (Paris) 245 (1957) 2063
58N1 Nickel, E.H., Rowland, J.F., Maxwell, J.A.: Can. Mineral. 6 (1958) 264
60B1 Barclay, G.A., Cox, E.G.: Z. Kristallogr. 113 (1960) 23
61N1 Nickel, E.H.: Am. Mineral. 51 (1961) 1549
61W1 Wilson, A., Leary, J.K.: Am. Mineral. 46 (1961) 759
62R1 Roy, D.M., Harker, R .I.: Int. Symp. Chem. Cem., Washington, 1960 p. 196; published in 1962
62S1 Shibayeva, K.I., Belov, N.V.: Dokl. Akad. Nauk SSSR 146 (1962) 128
62T1 Taylor, H.F.W.: Am. Mineral. 47 (1962) 932
63B1 Belov, N.V.: Crystal Chemistry of Large-Cation Silicates, Consultants Bureau, New York, 1963
65H1 Huang, Y.H.: Geol. Rev. 23 (1965) 7
65S1 Soloveva, L.P., Belov, N.V.: Sov. Phys. Crystallogr. 9 (1965) 458
66F1 Fleischer, M.: Am. Mineral. 51 (1966) 1546
66L1 Li Te-Yu, Simonov, V.I., Belov, N.V.: Sov. Phys. Dokl. Crystallogr. 11 (1966) 197
66P1 Portnov, A.M., Simonov, V.I., Sinyugina, G.P.: Dokl. Akad. Nauk SSSR 166 (1966) 119
67M1 McDonald, W.W., Cruickshank, D.J.W.: Z. Kristallogr. 124 (1967) 180
67R1 Roy, D.M., Johnson, D.M.: Proc. Autoclaved Calcium Silicate Building Products, London, 1965, p.114 (published 1967)
68F1 Fleischer, M.: Am. Mineral. 53 (1968) 348
70L1 Louisnathan, S.J., Smith, J.V.: Z. Kristallogr. 132 (1970) 288
71P1 Portnov, A.M., Krivokoneva, G.K., Stolyarova, T.I.: Zap. Vses. Mineral. Ova. 100 (1971) 599
72F1 Fleischer, M.: Am. Mineral 57 (1972) 1311
74A1 Aarden, H.M., Gittins, J.: Can. Mineral. 12 (1974) 241
74W1 Wieker, W.: in Neuere Ergebnisse der Anorganischen Chemie, Deutscher Verlag der Wissenschaften, Berlin, 1974, p. 238
76W1 Williams, S.A.: Am. Mineral. 61 (1976) 1255
77H1 Hill, R.J., Gibbs, G.V., Craig, J.R., Ross, F.K., Williams, J.M.: Z. Kristallogr. 146 (1977) 241
77S1 Saburi, S., Kawahara, A., Henmi, C., Kusachi, I., Kihara, K.: Mineral J. Sapporo 8 (1977) 286
78G1 Götz, J., Masson, C.R.: J. Chem. Soc. Dalton (1978) 1134
78T1 Takeuchi, Y., Sasaki, S., Joswig, W., Fuess, H.: Proc. Jpn. Acad. 54 (1978) 577
79K1 Krivokoneva, G.K. et al:: Dokl. Akad. Nauk SSSR Earth Sci. 248 (1997) 127
79M1 Mellini, M., Merlino, S.: Tschermaks Mineral. Petrogr. Mitt. 26 (1979) 109
80L1 Lippmaa, E., Magi, M., Samoson, A., Engelhardt, G., Grimmer, A.E.: J. Am. Chem. Soc. 102 (1980) 4889
81C1 Cooper, B.J., Gibbs, G.V., Ross, F.K.: Z. Kristallogr. 156 (1981) 305
81G1 Grimmer, A.R., Peter, R., Fechner, E., Molgedey, G.: Chem. Phys. Lett. 77 (1981) 331
81M1 Mellini, M.: Tschermaks Mineral. Petrogr. Mitt. 28 (1981) 99
83H1 Hamm, H.M., Hentschel, G.: Neues Jahrb. Mineral. Monatsh. (1983) 119
83R1 Raade, G., Mladeck, M.H.: Am. Mineral. 68 (1983) 1216
83S1 Smith, K.A., Kirkpatrick, B.J., Oldfield, E., Henderson, D.M.: Am. Mineral. 68 (1983) 1206
85H1 Hamilton, R.D., Finney, J.J.: Mineral. Mag. 49 (1985) 91
85V1 Vladykin, N.V., Drits, V.A., Kovalenko, V.I., Dorfman, M.D., Malov, V.S., Gorshkov, A.I.: Zap. Vses. Mineral. Ova. 114 (1985) 374
86A1 Al-Hermezi, H.K., McKie, D., Hall, A.J.: Mineral. Mag. 50 (1986) 119

86H1 Hawthorne, F.C., Fleischer, M., Grew, E.S., Grice, J.D., Jambor, J.L., Puziewicz, J., Roberts, A.C., Vanko, D.A., Zilczer, J.A.: Am. Mineral. 71 (1986) 127
86H2 Hazen, R.M., Au, A.Y.: Phys. Chem. Miner. 13 (1986) 69
87D1 Downs, J.W., Ross, F.K.: Am Mineral. 72 (1987) 97
87H1 Hawthorne, F.C., Bladh, K.W., Burke, E.A.J., Grew, E.S., Langley, R.H., Puciewicz, J., Roberts, A.C., Schedler, R.A., Shigley, J.E., Valko, D.A.: Am. Mineral. 72 (1987) 222
89M1 Mariano, A.N., Roeder, P.L.: Can. Mineral. 27 (1989) 709
89S1 Sarp, H., Peacor, D.R.: Am. Mineral. 74 (1989) 1203
91N1 Nickel, W.H., Nichols, M.C.: Mineral Reference Manual, Van Nostrand, Reinhold, 1991
95P1 Plaisier, J.R., Jansen, J., De Graaf, R.A.G., Ijdo, D.J.W.: J. Solid State Chem. 115 (1995) 464
97L1 Libowitzky, E., Rossman, G.R.: Eur. J. Mineral. 9 (1977) 793
97L2 Libowitzky, E., Kohler, T., Armbruster, T., Rossman, G.R.: Eur. J. Mineral. 9 (1997) 803